A&A 676, A126 (2023)
https://doi.org/10.1051/0004-6361/202346751

Astronomy & Astrophysics

Discovery and physical characterization as the first response to a potential asteroid collision: The case of 2023 DZ_2 ⋆,⋆⋆

Marcel M. Popescu[1,2], O. Văduvescu[3,4,5], J. de León[4,6], C. de la Fuente Marcos[7], R. de la Fuente Marcos[8], M. O. Stănescu[1,2], M. R. Alarcon[4,6], M. Serra Ricart[4,6], J. Licandro[4,6], D. Berteşteanu[1,2], M. Predatu[5], L. Curelaru[1], F. Barwell[3,9], K. Jhass[3,9], C. Boldea[5], A. Aznar Macías[10], L. Hudin[11], and B. A. Dumitru[12]

[1] Astronomical Institute of the Romanian Academy, 5 Cuţitul de Argint, 040557 Bucharest, Romania
e-mail: popescu.marcel1983@gmail.com
[2] Astroclubul Bucureşti, Blvd Lascăr Catargiu 21, 10663 Bucharest, Romania
[3] Isaac Newton Group of Telescopes (ING), Apto. 321, 38700 Santa Cruz de la Palma, Canary Islands, Spain
[4] Instituto de Astrofísica de Canarias (IAC), C/Vía Láctea s/n, 38205 La Laguna, Tenerife, Spain
[5] The University of Craiova, Str. A. I. Cuza nr. 13, 200585 Craiova, Romania
[6] Departamento de Astrofísica, Universidad de La Laguna, 38206 La Laguna, Tenerife, Spain
[7] Universidad Complutense de Madrid, Ciudad Universitaria, 28040 Madrid, Spain
[8] AEGORA Research Group, Facultad de CC. Matemáticas, Universidad Complutense de Madrid, Spain
[9] Department of Physics and Astronomy, University of Sheffield, Sheffield S3 7RH, UK
[10] Isaac Aznar Observatory, Alcublas, Valencia, Spain
[11] ROASTERR-1 observatory, Cluj-Napoca, Romania
[12] Institute of Space Science (ISS), 409, Atomiştilor Street, 077125 Măgurele, Ilfov, Romania

Received 26 April 2023 / Accepted 13 June 2023

ABSTRACT

Context. Near-Earth asteroids (NEAs) that may evolve into impactors deserve detailed threat assessment studies. Early physical characterization of a would-be impactor may help in optimizing impact mitigation plans. We first detected NEA 2023 DZ_2 on 27 February 2023. After that, it was found to have a minimum orbit intersection distance (MOID) with Earth of 0.00005 au as well as an unusually high initial probability of becoming a near-term (in 2026) impactor.
Aims. We perform a rapid but consistent dynamical and physical characterization of 2023 DZ_2 as an example of a key response to mitigating the consequences of a potential impact.
Methods. We used a multi-pronged approach, drawing from various methods (observational–computational) and techniques (spectroscopy–photometry from multiple instruments), and bringing the data together to perform a rapid and robust threat assessment.
Results. The visible reflectance spectrum of 2023 DZ_2 is consistent with that of an X-type asteroid. Light curves of this object obtained on two different nights give a rotation period $P = 6.2743 \pm 0.0005$ min with an amplitude $A = 0.57 \pm 0.14$ mag. We confirm that although its MOID is among the smallest known, 2023 DZ_2 will not impact Earth in the foreseeable future as a result of secular near-resonant behaviour.
Conclusions. Our investigation shows that coordinated observation and interpretation of disparate data provides a robust approach from discovery to threat assessment when a virtual impactor is identified. We prove that critical information can be obtained within a few days after the announcement of the potential impactor.

Key words. minor planets, asteroids: individual: 2023 DZ2 – techniques: spectroscopic – techniques: photometric – methods: observational – methods: numerical – celestial mechanics

1. Introduction

When a new Solar System body (asteroid or comet) is discovered and its observations cover a short time interval, the orbit determination has a large uncertainty. Thus, at a given moment, the object can be anywhere inside a region defined by the propagation of the orbital uncertainties. Milani et al. (2000) introduced the concept of virtual asteroid, a hypothetical object that follows any possible orbital solution obtained from the existing observations. If the dynamical evolution of any of these virtual asteroids is compatible with an Earth collision, this is called a virtual impactor (VI). Consequently, additional astrometric observations are needed to improve the orbit determination so the impact probability is better constrained, leading to its eventual removal as a threat (see e.g. Milani et al. 2000; Milani 2005). This can be accomplished either by triggering new telescope observations or by data-mining the various observatories databases for 'precoveries' (unnoticed apparitions in images acquired prior to its discovery), or both (see e.g. Vaduvescu et al. 2013, 2020).

⋆ Spectrum, spectro-photometric data, and light-curves are only available at the CDS via anonymous ftp to cdsarc.cds.unistra.fr (130.79.128.5) or via https://cdsarc.cds.unistra.fr/viz-bin/cat/J/A+A/676/A126

⋆⋆ Based on observations made with the Gran Telescopio Canarias (GTC) telescope and the Isaac Newton Telescope (INT), in the Spanish Observatorio del Roque de los Muchachos of the Instituto de Astrofísica de Canarias (programme IDs GTC31-23A and INT99-MULTIPLE-2/23A), and the Two-Meter Twin Telescope (TTT) and the Telescopio Carlos Sanchez (TCS), in the Spanish Observatorio del Teide of the Instituto de Astrofísica de Canarias (commissioning phase).

Large robotic surveys, such as the Panoramic Survey Telescope and Rapid Response System (Pan-STARRS; Kaiser 2004; Denneau et al. 2013), the Catalina Sky Survey (CSS; Christensen et al. 2012), the Asteroid Terrestrial-impact Last Alert System (ATLAS; Tonry et al. 2018), and the Zwicky Transient Facility (ZTF; Ye et al. 2019) are continuously discovering most of the near-Earth asteroids (NEAs) or near-Earth objects (NEOs) down to an apparent V magnitude as faint as 22 (depending on the survey). However, there are regions of the sky that may not be observed for a long time by these facilities, due to the observing strategy, the weather, instrument updates, or technical issues. Thus, the complementary observations performed by other facilities around the world are of significant importance for confirming, recovering, orbit refinement, and discovering NEOs.

The efficiency in finding unknown Solar System objects (SSOs) depends on two factors, the limiting magnitude that can be reached with an instrument and the sky area that can be covered. Because the majority of the facilities whose aim is to find NEAs do not have access to telescopes with large aperture (compared with those of the above-mentioned surveys), a wide field of view (FoV) covered during an observing run remains the accessible option. For example, an ingenious approach is used by Alain Maury, Georges Attard, Daniel Parrott, and their collaborators (the team of the MAP telescopes) to survey the Southern sky with small-aperture telescopes having a large FoV[1].

Close passers are small bodies that experience periodic close encounters with the Earth-Moon system and may eventually collide with Earth. Considering geological timescales, these small bodies represent a potential threat to life on our planet. This is evidenced by past impact events such as superbolides, known craters, and mass extinctions attributed to major impacts. According to the most recent work, there are at least 210 known Earth craters caused by asteroids or comets (Kenkmann & Artemieva 2021; James et al. 2022), while, on average, every year one meteoroid of about 3–4 m explodes in the atmosphere of our planet (see e.g. Devillepoix et al. 2019).

The Chelyabinsk superbolide fall on 15 February 2013 reminded us that collisions of small Solar System bodies with Earth may have catastrophic consequences (Brown et al. 2013; Borovička et al. 2013). Despite the relatively small size of this asteroid (about 18 m) that entered through the atmosphere on that date, it caused a significant amount of ground damage due to the air burst, affecting an area of more than 10 000 km^2 and causing injuries to more than 1500 people (see e.g. Kartashova et al. 2018). This small NEA was not detected by active surveys because its apparent motion was too close to the Sun prior to impact. Thus, no mitigation measurements were attempted.

In order to mitigate these natural disasters, it is critical that these NEOs are first discovered with sufficient time prior to impact, and then their physical properties are determined as accurately and rapidly as possible. For example, metallic asteroids may overcome current asteroid impact avoidance strategies and survive after falling through the atmosphere causing major damage when they collide with our planet. The measures to prevent the impact or mitigate its consequences can only be taken based on information gained from detailed telescopic observations. The capability to offer a rapid response to a potential danger is a key factor for proper mitigation. Early physical characterization of a would-be impactor may help in optimizing impact mitigation plans.

[1] https://www.spaceobs.com/en/Alain-Maury-s-Blog/2023-DW accessed on 22 April 2023.

Table 1. Values of the heliocentric Keplerian orbital elements and their respective 1σ uncertainties of 2023 DZ$_2$.

Orbital parameter		Value$\pm1\sigma$ uncertainty
Semi-major axis, a (au)	=	2.1555715±0.0000002
Eccentricity, e	=	0.53892721±0.00000005
Inclination, i (°)	=	0.0814345±0.0000012
Longitude of the ascending node, Ω (°)	=	187.91380±0.00006
Argument of perihelion, ω (°)	=	5.95978±0.00006
Mean anomaly, M (°)	=	348.674236±0.000002
Perihelion distance, q (au)	=	0.993875393±0.000000007
Aphelion distance, Q (au)	=	3.3172677±0.0000003
Absolute magnitude, H (mag)	=	24.3±0.4

Notes. The orbit determination of 2023 DZ$_2$ is referred to epoch JD 2460000.5 (25 February 2023) TDB (Barycentric Dynamical Time, J2000.0 ecliptic and equinox) and it is based on 635 observations with a data-arc span of 72 days (solution date, 24 April 2023, 08:41:00 PDT). The input data also include radar observations (4 delay and 1 Doppler). Source: JPL SBDB.

A recent example of this sequence of events at work is represented by 2023 DZ$_2$. We discovered this Apollo-class NEA on the night of 27 February 2023 using the 2.54 m *Isaac Newton* Telescope (INT)[2] within the context of the EUROpean Near Earth Asteroids Research (EURONEAR) collaboration[3]. We promptly followed up this discovery with astrometric observations during the next two nights. The data were submitted to the Minor Planet Center (MPC)[4]. Immediately after the announcement of its discovery through an Minor Planet Electronic Circular (MPEC 2023-F12, Vaduvescu et al. 2023), it was catalogued as a VI by the Jet Propulsion Laboratory (JPL) Sentry System for Earth impact monitoring[5], by the NEODyS CLOMON2 Risk page[6] list, and also by ESA Risk List[7]. As additional observations were reported to the MPC by multiple observers around the world, the cumulative impact probability increased by several orders of magnitude (up to a cumulative impact probability of 0.0023 on 18 March), but the analysis of the improved orbits led to the eventual removal of 2023 DZ$_2$ from the Sentry System on 21 March.

Based on the apparent magnitude values reported together with the astrometric measurements by various observers, an absolute magnitude $H \approx 24$ was estimated, which indicates a size in the range of 40 m to 100 m. A potential impact of such an asteroid can cause damage at the local or regional level (see e.g. Morrison 1992). A close approach date of 25 March 2023 was estimated. As this NEA became brighter, more observations were reported including many by amateur astronomers who were able to acquire highly accurate data with affordable equipment (e.g. Farnocchia et al. 2022; Bertești eanu et al. 2022). Fortunately, the impact probability decreased at insignificant levels ($\approx 10^{-7}$) during the following days. The orbital elements of 2023 DZ$_2$ derived by using 634 observations with a data-arc covering 72 days are reported in Table 1.

Nevertheless, 2023 DZ$_2$ safely passed at a distance of 175 030 km from Earth on March 25 at 19:51 TDB (timescale conversion difference TDB − UT 69.185285 s), when it reached

[2] https://www.ing.iac.es/astronomy/telescopes/int/
[3] http://www.euronear.org
[4] https://www.minorplanetcenter.net/iau/mpc.html
[5] https://cneos.jpl.nasa.gov/sentry/
[6] https://newton.spacedys.com/neodys/index.php?pc=4.0
[7] https://neo.ssa.esa.int/risk-list

Table 2. Observational circumstances of 2023 DZ_2.

Obs. type	Date Obs. (UTC)	m_V	α (°)	Δ (au)	r (au)
Phot.	2023 03 20.9143	18.0	60.5	0.021	1.006
	2023 03 21.9284	17.5	60.9	0.017	1.004
	2023 03 22.9467	16.8	60.8	0.013	1.003
Colo.	2023 03 22.8725	17.0	60.7	0.013	1.003
Spec.	2023 03 17.8739	19.0	57.9	0.034	1.013
	2023 03 20.9161	18.0	60.5	0.021	1.006

Notes. Observation type includes time-series photometry (Phot.), colour photometry (Colo.), and visible spectra (Spec.). The UTC time corresponding to the start of the observations, the predicted apparent V magnitude (m_V), the phase angle (α), and the geocentric(Δ) and heliocentric (r) distances are shown (obtained using the MPC ephemeris service accessed on 30 March 2023).

an apparent visual magnitude of 10.3 (for a minimum of ≈10 mag reached about 2 h prior to perigee). Thanks to its brightness, it offered a unique opportunity for characterization via various observational techniques: photometry, spectro-photometry, spectroscopy of various spectral intervals (visible, near-infrared, mid-infrared), polarimetry, and radar.

The International Asteroid Warning Network (IAWN)[8] organized a world-wide campaign with the aim of involving as many observing facilities as possible, in a coordinated manner, to obtain the most accurate physical information about this object. This international organization was established in 2013 as a result of the UN-endorsed recommendations for an international response to a potential NEO impact threat. Their objective is to develop a strategy using well-defined communication plans and protocols to assist Governments in the analysis of asteroid impact consequences and in the planning of mitigation responses.

The close approach of 2023 DZ_2 offered a great opportunity for a world-wide collaboration to study a potential NEA impactor discovered one month prior to its close approach. Previous IAWN campaigns (Reddy et al. 2019, 2022; Farnocchia et al. 2022) targeted NEAs discovered some years before, thus allowing plenty of time to organize them.

In this paper, we show the results of our observing campaign, performed using several telescopes from the observatories of the Canary Islands whose aim was to determine the physical properties of 2023 DZ_2. The objective of our work is to highlight the critical observational capabilities, both in terms of instruments and data analysis resources, required to implement mitigation strategies to face the potential disasters coming from a cosmic hazard such as an asteroid impact.

In less than a week from the announcement of the discovery and initial classification as VI of 2023 DZ_2, we were able to determine its spin rate and the light curve amplitude, its visible colours, and to obtain its visible spectrum. The observations performed are shown in Table 2. Based on these observational data, we were able to constrain its size and estimate its composition. In addition, we were able to predict reliably its dynamical evolution in the time interval (−47, +142) yr. This paper is organized as follows. In Sect. 2, we present the observations of 2023 DZ_2 and the methods used for its detection. The dynamical evolution is discussed in Sect. 3. In Sect. 4, we present the photometric observations and the spin properties. The results of the analysis of the spectro-photometric data and the spectra are shown in Sect. 5. The discussion and the conclusions are shown in Sect. 6. Additional data obtained within the framework of our collaboration of professional and amateur astronomers (known as Pro-Am) are discussed in Appendix A.

2. The detection of 2023 DZ_2

The traditional way of finding new NEAs in CCD frames is the blinking detection technique. It begins with sequences of a few consecutive images in the same area of the sky, acquired with the same exposure parameters (e.g. exposure time, gain) during several tens of minutes. The raw images are processed and aligned using the stars in the field, so that any moving source (asteroid) appears to shift within the acquired image sequence. Assuming a linear motion in the short time interval covered by the observations, most of the noise can be identified and rejected; the targets are then validated, and their measurements reported to the MPC. In the early days of NEA surveys, a human operator manually performed most of these tasks. A popular representative example implementation of this technique, often applied two decades ago, involved the use of the Astrometrica software[9]. With the advent of the all-sky surveys dedicated to the discovery of SSOs, more advanced detection software packages were developed (Denneau et al. 2013).

Even the largest telescopes available cannot detect fainter and faster asteroids (as is the case with most NEAs) through the blink method, due to atmospheric effects, mostly air glow (e.g. skyglow, light pollution) and dispersion, and detector limitations. If a known object is invisible in the individual images, it is still possible to recover it through a technique called track-and-stack. Multiple exposures are taken, which are shifted based on the predicted direction and speed of the target, and then stacked to improve the signal-to-noise ratio (S/N), allowing the object to be detected with certainty in the co-added image. This technique makes sense for cases where the telescope does not support tracking an object itself (non-sidereal tracking) or when the trajectory is known only after acquiring the exposures. Otherwise, it is possible to just track according to the SSO apparent motion and then take a long exposure.

There is a natural extension of this method to the detection of unknown SSOs called synthetic tracking (also known as digital tracking). It was used to search for very faint Kuiper belt objects (KBOs) and trans-Neptunian objects (TNOs), which move very slowly (Cochran et al. 1995; Gladman & Kavelaars 1997; Gladman et al. 1998). As suggested by its name, this method applies track-and-stack to synthetic motion vectors, typically all plausible motion vectors, while scanning for detections. However, practical synthetic tracking algorithms operate differently from track-and-stack; the detection algorithm performs the stacking, and it must identify automatically the unknown object since the number of resulting stacked images is impossible to analyse in practical time by human validators.

The key factor for all these techniques is the time needed for the data reduction because the small close-approaching NEAs are only observable (at apparent magnitudes accessible with ground-based telescopes) for very short time intervals. While modern instruments cover larger fields of view (already of the order of several square degrees) with fainter magnitude limits, the effort needed to reduce the amount of data collected becomes prohibitive for small research groups or amateurs. Thus, fast and accurate algorithms are required to complement the ongoing robotic all-sky surveys carried out by large research consortia

[8] https://iawn.net/

[9] http://www.astrometrica.at/

Table 3. Observational circumstances for the detection of 2023 DZ_2.

Field name	Date	UT start	UT end	Nexp	AM	Seeing
n1o1	27-Feb.-2023	22:21	23:31	12	1.02	1.5
E309252	28-Feb.-2023	22:14	22:28	12	1.01	1
E309252	01-Mar.-2023	22:46	22:00	12	1.02	1.1

Notes. The date and Universal Time (UT) for the beginning and for the end of the observing set, the number of exposures (NExp), the mid-observation airmass (AM), and the median seeing (Seeing) in arcseconds are shown.

(e.g. Pan-STARRS, CSS, ATLAS, ZTF). One successful example of such a software application is Tycho Tracker[10], which is used by both amateur and professional astronomers. This software provides an easy-to-use interface that facilitates the detection and measurement of asteroids, comets, and variable stars. It also supports the synthetic tracking technique. However, the integration of this software in an automatic data reduction pipeline is not straightforward, and the computation power required to search for fast-moving NEAs in a large field of view increases exponentially.

Within the EURONEAR collaboration, we started the development of Synthetic Tracking on Umbrella (STU), a synthetic tracking pipeline that aims to run in near real time with the observations. It is a new addition to the Umbrella software suite (Stănescu & Văduvescu 2021) and it uses OpenCL to tap into the power of modern graphics processing unit (GPU). As a pipeline, STU begins with image conditioning tasks, such as star masking (median stacking and star detection/mask generation through Umbrella2, handled on the central processing unit (CPU), masking the original images through OpenCL on the GPU).This is followed by re-projecting the input images into a common gnomonic projection chart (so that asteroids move, to first approximation, in straight lines in X-Y coordinates) directly on the GPU (Stănescu et al. 2023).

The data cube is then processed in 'scan stage', which is the actual GPU-based search. The search algorithm applies a combination of threshold counting (Yanagisawa et al. 2021), a generalization of thresholding the median value that is very robust against false positives, with the more common addition described by Whidden et al. (2019) for refining the results (since computing the median is expensive, and threshold counting does not provide additional information for bright targets).

Thus, we first detected 2023 DZ_2 (Vaduvescu et al. 2023) thanks to the real-time processing using the software tools and infrastructure of the Romanian ParaSOL project[11]. Table 3 summarizes the observing log. The objective of the observing run was to prove the near-real-time capabilities of the developed software, including STU, sensor correction, and the plate solving pipeline. Nevertheless, this serendipitous discovery was made within the framework of our observing campaigns whose aim is finding new asteroids and comets (NEAs, Atiras, and Vatiras). The observing strategy was designed to cover the sky regions where it is more likely to detect unknown NEAs (by exploring ranges of ecliptic longitude neglected by the main surveys).

The detection was found in CCD3 (Fig. 1) of the Wide Field Camera (WFC) mounted at the prime focus of the INT, an optical mosaic imaging instrument made of four charge-coupled devices (CCDs). They cover 0.27 square degrees arranged in a 34×34 arcmin^2 L-shaped design with about 17–22 arcsec gaps between CCDs. The object was identified at an apparent magnitude of 20.3 (in the G band), and it was validated in all stacked images (using the mean, median, trimmed mean, and masked trimmed mean methods) generated as output (Stănescu et al. 2023).

For the new detection corresponding to 2023 DZ_2, STU reported an average rate of apparent motion on sky of 0.7326 arcsec min^{-1} (−0.777 arcsec min^{-1} in RA, 0.066 arcsec min^{-1} in DEC, on coordinate motion) for an average position angle of 274.°6. The object was also independently detected using the Tycho tracker software by one of our ParaSOL collaborators. In order to confirm it, we performed a final check of the images using the Astrometrica software[12] (the object was detectable in the single exposures). The future releases of our STU pipeline will focus on achieving and proving the real-time candidate validation and reporting capabilities of the software developed within the ParaSOL project. Although in this case only 12 images were obtained during each observing night, the synthetic tracking algorithm allowed us to detect the object automatically in near real time.

3. Dynamics

Asteroid 2023 DZ_2 has a minimum orbit intersection distance (MOID) with Earth of 0.00005 au, one of the lowest known among NEAs. This means that the intersection point between its orbit and the invariable plane is very close to the path of the Earth–Moon system and that encounters at 1.17 Earth radii are theoretically possible in the absence of protective mechanisms such as mean-motion or secular resonances. The nominal evolution of the orbit of 2023 DZ_2 as predicted by the JPL `Horizons` online Solar System data and ephemeris computation service[13], is shown in Fig. 2, left panels. The orbital evolution shows multiple discontinuities linked to past and future close encounters of 2023 DZ_2 with the Earth–Moon system.

Table 1 shows that the perihelion of 2023 DZ_2 takes place in close proximity to Earth's orbit, while its aphelion occurs close to the core region of the main asteroid belt. Its semi-major axis at 2.15 au is in the region associated with the $\nu 6$ secular resonance in which the value of the longitude of perihelion ($\varpi = \Omega + \omega$; see e.g. Murray & Dermott 1999) of a minor body relative to that of Saturn oscillates about 0° or 180° (see e.g. Froeschle & Scholl 1989; Morbidelli & Henrard 1991). This is the secular apsidal resonance with Saturn. Figure 2, centre panels, shows the nominal evolution of the critical angle associated with the apsidal resonances of 2023 DZ_2 with Venus, Earth, Mars, Mercury, Jupiter, and Saturn. While 2023 DZ_2 is not currently subjected to the $\nu 6$ secular resonance, it appears to have been subjected to the $\nu 5$ secular resonance with Jupiter in the recent past. As the associated critical angle librated about 180° (see Fig. 3), 2023 DZ_2

[10] https://www.tycho-tracker.com/
[11] https://planet.astro.ro/ParaSOL/
[12] http://www.astrometrica.at/
[13] https://ssd.jpl.nasa.gov/horizons/

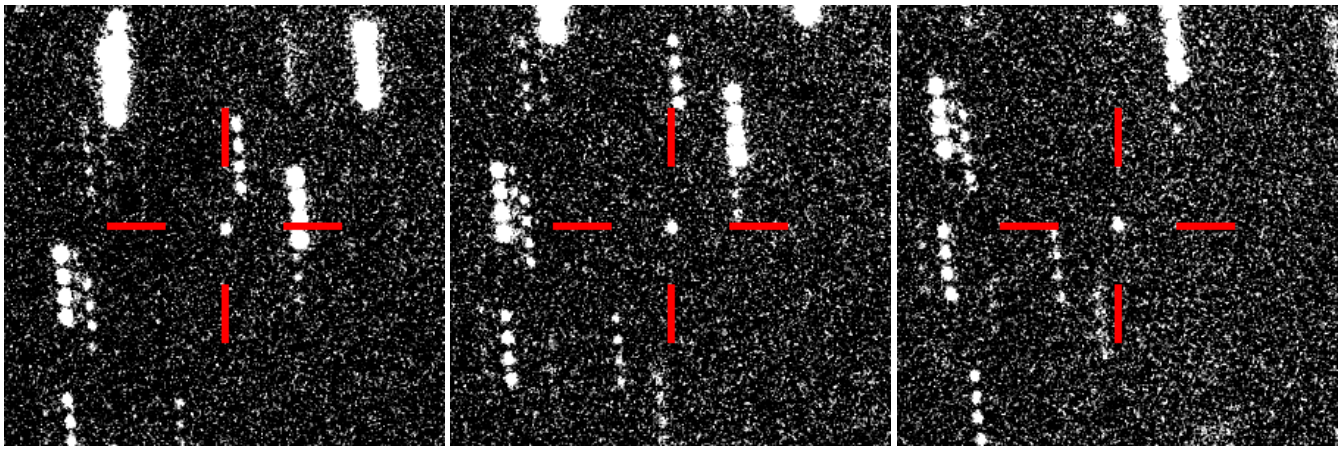

Fig. 1. Re-scaled mean combined images used to detect 2023 DZ_2 by the STU algorithm. Three subsets of four images each were stacked to detect this new object.

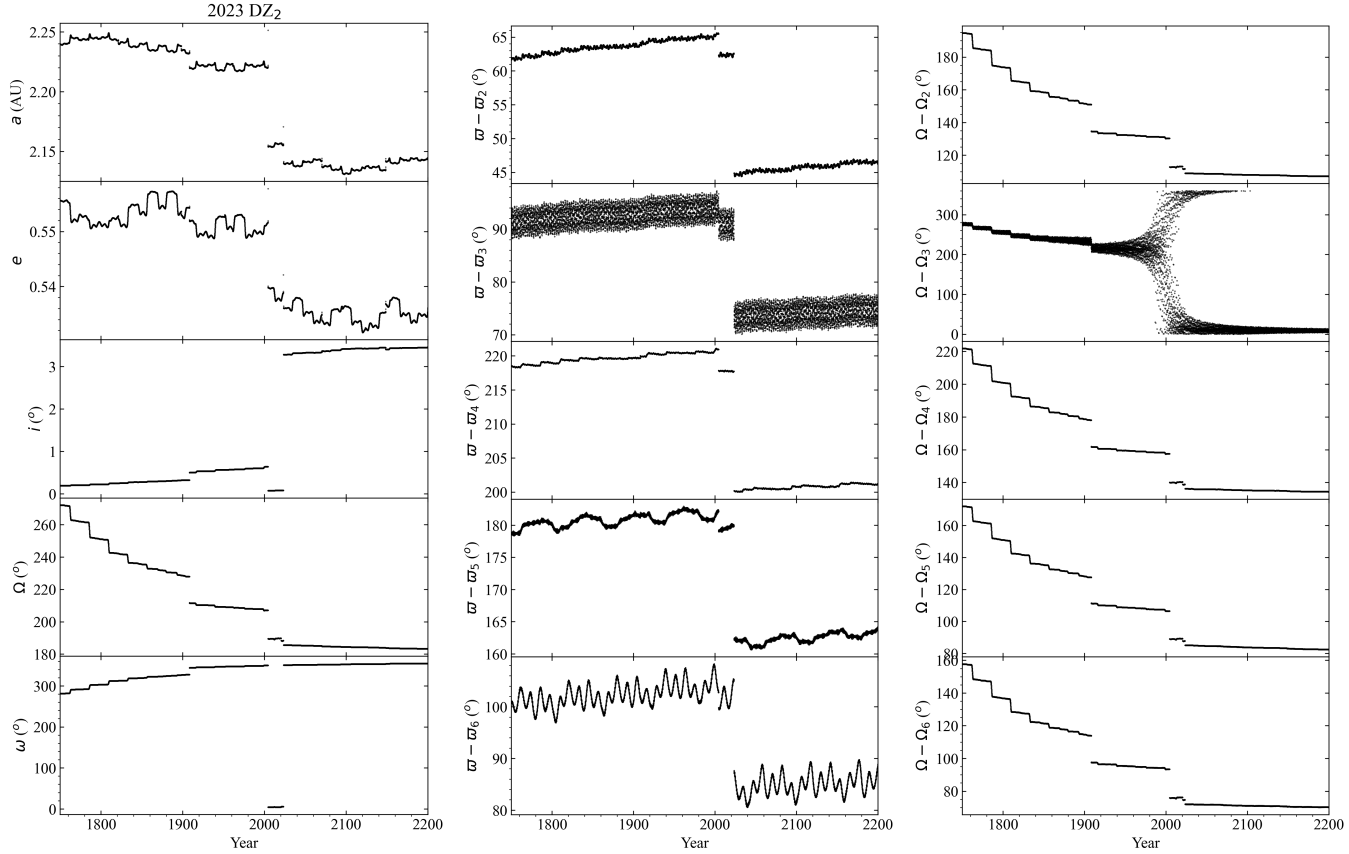

Fig. 2. Relevant dynamical evolution of 2023 DZ_2. *Left panels*: short-term orbital evolution of 2023 DZ_2: a, semi-major axis (top panel); e, eccentricity (second to top panel); i, inclination (centre panel); Ω, longitude of the ascending node (second panel from bottom); and ω, argument of perihelion (bottom panel). *Centre panels*: longitude of perihelion of 2023 DZ_2, $\varpi = \Omega + \omega$, relative to that of Venus (ϖ_2, top panel), Earth (ϖ_3, second to top panel), Mars (ϖ_4, centre panel), Jupiter (ϖ_5, second panel from bottom), and Saturn (ϖ_6, bottom panel). An apsidal secular resonance leads to the libration of the angle $\varpi - \varpi_i$ about a constant value (0° or 180°). *Right panels*: longitude of the ascending node relative to that of Venus (Ω_2, top panel), Earth (Ω_3, second to top panel), Mars (Ω_4, centre panel), Jupiter (Ω_5, second panel from bottom), and Saturn (Ω_6, bottom panel). A nodal secular resonance occurs when the angle $\Omega - \Omega_i$ librates about a constant value. The evolution shown here is based on the nominal orbit in Table 1 and the output cadence is 15 days. Data source: JPL `Horizons`.

reached aphelion when Jupiter was at perihelion. This explains why the MOID of 2023 DZ_2 with Jupiter amounts to 1.636 au. On the other hand, Fig. 2, right panels, reveals that 2023 DZ_2 is in nearly nodal resonance with Earth as the ascending node of this small body is in the path of our planet.

In summary, the dynamics of 2023 DZ_2 is controlled by Earth and Jupiter, with Earth currently being a direct perturber as a result of the near nodal resonance and Jupiter playing the role of secular perturber that projected a near apsidal resonance on 2023 DZ_2. The fact that this object is not subjected

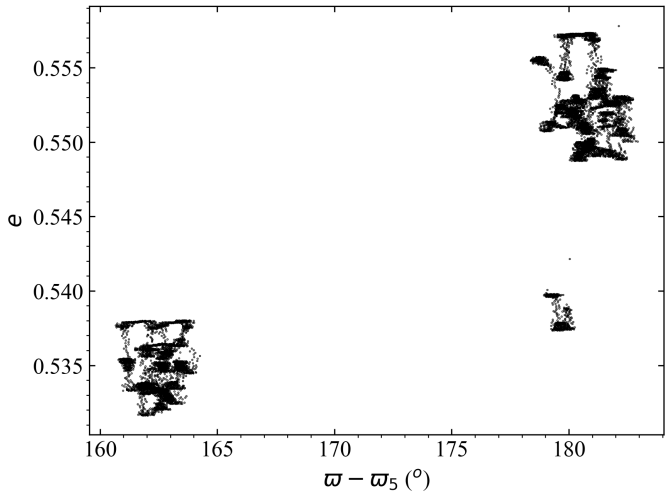

Fig. 3. Eccentricity vs $\varpi - \varpi_5$ for 2023 DZ_2.

to the $\nu 6$ secular resonance could explain why its MOID with Earth is so small and yet its probability of impact in the near future is zero. We may argue that NEA 2023 DZ_2 was somewhat protected against collision with Earth by a near $\nu 5$ secular resonance. The data discussed above were retrieved from the JPL Small-Body Database (SBDB)[14], which is provided by the Solar System Dynamics Group (SSDG, Giorgini 2011, 2015)[15], and `Horizons` using tools provided by the `Python` package `Astroquery` (Ginsburg et al. 2019) and its `HorizonsClass` class[16].

The analysis above tells us nothing about the role of the uncertainties on the computed evolution of this NEA, but relatively large uncertainties coupled with recurrent encounters at close range may severely hamper our ability to explore the orbital evolution of this object beyond a few decades from the current epoch (see e.g. Valsecchi et al. 2003). In order to investigate the role of the uncertainties on the reconstruction of the past evolution of this NEA and on the prediction of its future behaviour, we performed N-body simulations using a direct N-body code developed by Aarseth (2003) that implements the Hermite integration scheme formulated by Makino (1991). The code is publicly available from the website of the Institute of Astronomy of the University of Cambridge[17]. Relevant results from this code were discussed in detail in de la Fuente Marcos & de la Fuente Marcos (2012), which also includes many technical details.

Figure 4 shows our results for the orbital evolution of the nominal orbit of 2023 DZ_2 in the time interval (−10 000, 10 000) yr around the standard epoch JD 2460000.5 (25 February 2023) TDB that is the origin of times in the figure. The enhanced probability of encounters at close range is connected to the fact that the nodal distances experience an oscillation that periodically places the nodes of 2023 DZ_2 in the path of Earth (Fig. 4, bottom panel). On the other hand, the value of the Kozai–Lidov parameter (Fig. 4, second to top panel) does not experience obvious oscillations, and we can discard that 2023 DZ_2 could be subjected to a von Zeipel–Lidov–Kozai secular resonance (von Zeipel 1910; Lidov 1962; Kozai 1962; Ito & Ohtsuka 2019).

[14] https://ssd.jpl.nasa.gov/tools/sbdb_lookup.html#/
[15] https://ssd.jpl.nasa.gov/
[16] https://astroquery.readthedocs.io/en/latest/jplhorizons/jplhorizons.html
[17] http://www.ast.cam.ac.uk/ sverre/web/pages/nbody.htm

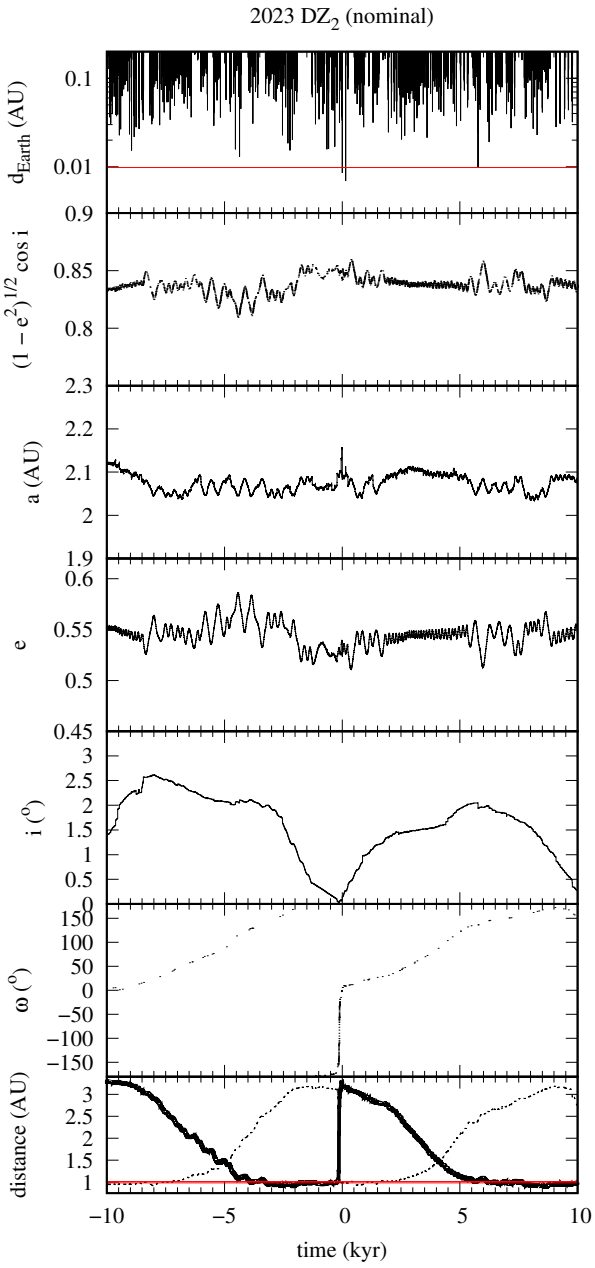

Fig. 4. Evolution over time of orbital elements and other relevant parameters for the nominal orbit of 2023 DZ_2 (see Table 1). The top panel shows the evolution of the geocentric distance; the value of the Hill radius of the Earth, 0.0098 au, is plotted as reference. The second to top panel focuses on the evolution of the value of the Kozai–Lidov parameter. The following four panels show the evolution of the values of semi-major axis, eccentricity, inclination, and argument of perihelion of the nominal orbit. The bottom panel displays the distances from the descending (thick line) and ascending nodes (dotted line) to the Sun; Earth's aphelion and perihelion distances are shown in red. The output time-step size is 0.1 yr. The source of the input data is JPL SBDB. The standard epoch JD 2460000.5 (25 February 2023) TDB, which is the origin of times.

Figure 5 shows the short-term evolution of control orbits with initial conditions separated from those of the nominal orbit. From the calculations, we find that predicting the future evolution of this NEA becomes difficult after 12 April 2165, when 2023 DZ_2 will experience another encounter with Earth, this time at 0.01 au. Investigating its orbital past is also challenging

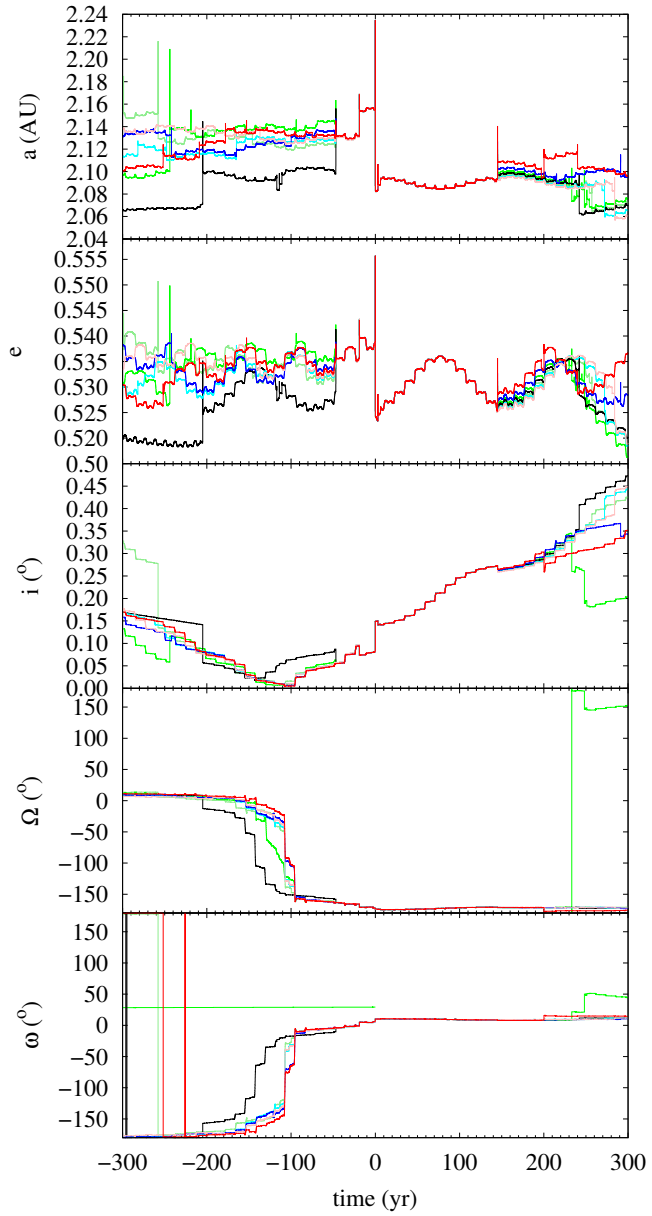

Fig. 5. Evolution of the values of the semi-major axis (a, top panel), eccentricity (e, second to top panel), inclination (i, third to bottom panel), ascending node (Ω, second to bottom panel), and argument of perihelion (ω, bottom panel) of 2023 DZ_2. The panels display the results of integrations for the nominal orbit (in black) and those of control orbits with Cartesian vectors separated $\pm3\sigma$ (in light green, -3σ, and green, 3σ), $\pm6\sigma$ (in cyan, -6σ, and blue, 6σ), and $\pm9\sigma$ (in pink, -9σ, and red, 9σ). The output time-step size is 4.383 h. The source of the input data is JPL SBDB and they are referred to the standard epoch JD 2460000.5 (25 February 2023) TDB, which is the origin of times.

because a relatively distant encounter with Jupiter on 17 March 1976 placed the object in its present trajectory. Between these two dates, all the control orbits up to $\pm9\sigma$ from the nominal solution provide a consistent picture of the orbital evolution of this NEA.

So far we have included the uncertainties by assuming that they are uncorrelated. This is a valid assumption when the orbit determination is robust, based on a large number of high-quality observations spanning a long time interval. However, this is not the case for 2023 DZ_2. In order to account for any correlations

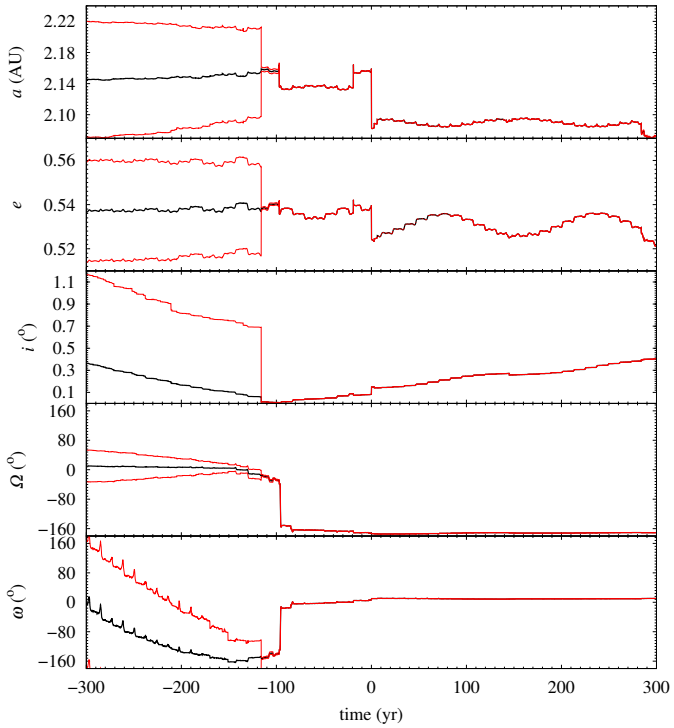

Fig. 6. Evolution of the values of the semi-major axis (a, top panel), eccentricity (e, second to top panel), inclination (i, third to bottom panel), ascending node (Ω, second to bottom panel), and argument of perihelion (ω, bottom panel) of 2023 DZ_2 according to the MCCM approach. The panels display the results of the integrations of 10^3 control orbits with initial positions and velocities generated using the MCCM methodology. In black is the average evolution of the orbital element and in red the range linked to the 1σ uncertainty or the 16th and 84th percentiles. The output time-step size is 0.1 yr. The source of the input data is JPL SBDB and they are referred to epoch 2460023.5 (20 March 2023) TDB, which is the origin of times.

present in the data, we carried out additional integrations backward and forward in time using initial conditions corresponding to control or clone orbits produced by the Monte Carlo using the Covariance Matrix (MCCM) approach described by de la Fuente Marcos & de la Fuente Marcos (2015). These synthetic orbits are based on the nominal orbit determination (see Table 1) with random noise added on each orbital element by making use of the covariance matrix. The covariance matrix was retrieved from the JPL SSDG SBDB using the `Python` package `Astroquery` and its `SBDBClass`[18] class, and is referred to epoch 2460023.5 (20 March 2023) TDB, which is the origin of times for the new calculations. The MCCM methodology was used to generate initial positions and velocities for 10^3 control orbits that were evolved dynamically using the direct N-body code.

Figure 6 shows the result of the past and future evolution of 2023 DZ_2 according to the MCCM approach. In black we display the average evolution and in red we show the range linked to the 1σ uncertainty or the 16th and 84th percentiles. While the uncertainty in the reconstruction of the past orbital evolution of this NEA is large beyond 100 yr into the past, that associated with the predictions of its future orbital behaviour is far smaller. This is the result of particularly close encounters with the Earth–Moon system when the orbital inclination of 2023 DZ_2 became virtually zero, over one century ago. Therefore, its current orbit

[18] https://astroquery.readthedocs.io/en/latest/jplsbdb/jplsbdb.html

determination is not robust enough to investigate its origin and how this object was inserted in NEA orbital parameter space. More observations are needed to produce a better orbit determination for such a study. On the other hand, our results based on the covariance matrix are quite consistent with those obtained assuming uncorrelated uncertainties.

4. Time-series photometry

Photometric data were obtained during three consecutive nights at the Telescopios Gemelos de Dos Metros (Two-meter Twin Telescope, TTT) facility. This is located at the Teide Observatory (latitude: 28°18′01.8″ N; longitude: +16°30′39.2″ W; altitude: 2386.75 m), on the island of Tenerife (Canary Islands, Spain). Currently, it includes two telescopes (called TTT1 and TTT2) with an aperture of 0.80 m, installed on altazimuth mounts, and with focal ratios of f/4.4 and f/6.8, respectively.

The observations were made using the QHY411M[19] cameras (Alarcon et al. 2023) installed on one of the Nasmyth ports of each telescope. They are equipped with scientific Complementary Metal–Oxide–Semiconductor (sCMOS) image sensors consisting of 151 megapixels with a pixel size of 3.76 µm pixel^{-1}. This provides an effective FoV of 51.4′×38.3′ (with an angular resolution of 0.22″ pixel^{-1}) in TTT1 and 33.1′×24.7′ (angular resolution of 0.14″ pixel^{-1}) in TTT2. In all the observing runs a band-pass filter was used; the band covers the 0.4–0.7 µm wavelength interval. The exposure time was dynamically set between 10 and 20 s to ensure a S/N higher than 50. A total of five observing runs were performed, one with TTT2 on 20 March and two simultaneous runs with each telescope on the nights of 21 and 22 March. Table 2 shows the effective coverage time for each night.

The images were bias and sky flat-field corrected. Then they were trimmed and binned at 2×2. Aperture photometry was performed using Tycho Tracker software. The images were aligned with bicubic interpolation and down-sampled by a factor of 2 for astrometric calibration, which was performed with Astrometry.net (Lang et al. 2010).

To obtain the photometry of the object, a fixed aperture of 2× full width at half maximum (FWHM) of the point spread function of stars in the first image of each set was used. An outer ring with the inner radius located at 4×FWHM was used to estimate the sky background signal. The same apertures were used for the comparison stars, selected constraining $0.60 < (B - V) < 0.70$. The initial and final positions of the asteroid were marked manually in the images in order to prevent any misidentification by the algorithm.

Photometric measurements were extracted and corrected for distance and light-time. The five-term Lomb–Scargle periodogram was obtained, with a well-marked peak in the power spectrum centred at a period of $P_{\rm rot} = 6.2743 \pm 0.0005$ min and its aliases. As uncertainty, 1σ of the Gaussian curve fitted to the exponentiated power peak was taken (VanderPlas 2018). The phased light curve is shown in Fig. 7. The amplitude of the curve obtained, considering photometric errors, is 0.57 ± 0.14 mag.

The initial observations performed with TTT1 and TTT2 show a super-fast rotator asteroid (Licandro et al. 2023). The $P_{\rm rot} = 6.274$ min is indicative of intrinsic strength to resist centrifugal disruption, otherwise 2023 DZ$_2$ would break apart (Pravec & Harris 2000). It could be a coherent body or monolith (e.g. Monteiro et al. 2020; Sánchez & Scheeres 2014). The data existing in the Asteroid Lightcurve Database (LCDB, Warner et al. 2009)[20], updated in February 2023, shows that no faster rotator corresponds to a low-albedo (i.e. ≤0.10) asteroid (Licandro et al. 2023). Thus, at first glance, the period determination adds a strong constraint to the cohesive strength of the asteroid, and it is a strong indicative of a high-albedo asteroid.

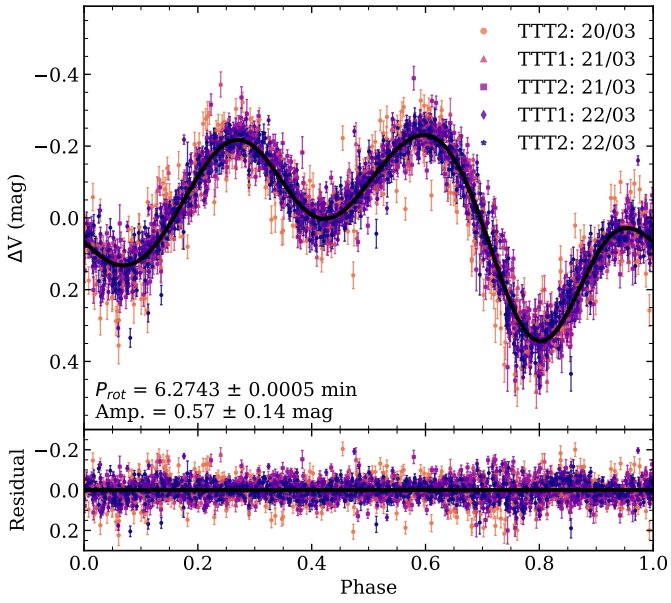

Fig. 7. Phased light curve of 2023 DZ$_2$ computed from photometric measurements obtained by TTT1 and TTT2. The rotation period and amplitude of the curve are shown in the lower left corner of the top panel. The total coverage is 9.8 h, distributed over three consecutive nights. Residuals are shown in the bottom panel.

The hypothesis of a high-albedo object is supported by the spin limit for small asteroids (Monteiro et al. 2020; Rondón et al. 2020). At an absolute magnitude $H \approx 24$ mag and an albedo of $p_V \leq 0.1$, this asteroid will have a size larger than 60 m, which for a rotation period of $P_{\rm rot} = 6.2743 \pm 0.0005$ min is outside the spin barrier determined by Rondón et al. (2020) for C-type asteroids.

The three peaks of the light curve show an irregular shape, which favours the hypothesis of a monolithic body. This result was confirmed by observations performed on 25 March with the Goldstone Radar. The preliminary result reported on their webpage[21] shows that 'at some orientations the shape looks somewhat triangular; at others it looks rounded; there is a flat area, and a small-scale topographic feature that appears on the leading edge'.

5. Spectro-photometry and spectroscopy

The spectro-photometric (photometric observations performed with various broad-band filters) and the spectral observations represent the best ground-based observing techniques to constrain the composition properties of small objects. The spectro-photometric method is more suitable for characterizing fainter objects since the incoming flux is collected in each bandpass and not dispersed as in the case of spectral observations. The faintest targets, which cannot be spectroscopically observed with any other telescope, can be taxonomically classified using this technique. The disadvantage is the impossibility of making a

[19] https://www.qhyccd.com/

[20] https://minplanobs.org/mpinfo/php/lcdb.php

[21] https://echo.jpl.nasa.gov/asteroids/2023DZ2/2023DZ2.2023.goldstone.planning.html

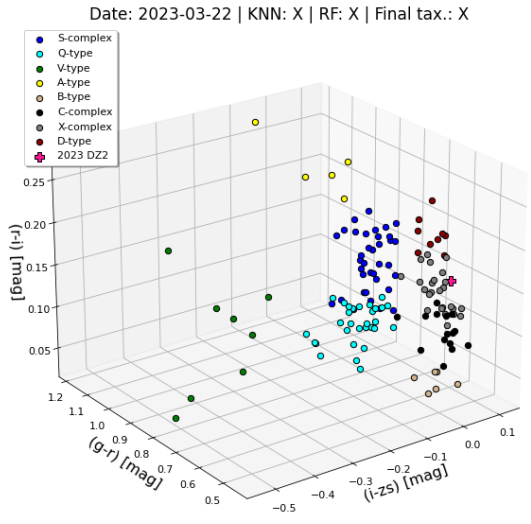

Fig. 8. Colour–colour diagrams, $(g - r)$ vs. $(r - i)$ vs. $(i - z_s)$, of the 155 objects with known spectral classification, used to classify 2023 DZ_2 based on the TCS/MusSCAT2 data. The taxonomic types defined in the DeMeo et al. (2009) system are divided into three major composition groups: the Q/S-complex (green and blue dots), the C-complex (black dots), and the X-complex (grey dots). In addition, three end-member types are considered: A-, D-, and V-type.

distinction between different sub-types of the same taxonomic complex. This is because a colour is just the normalized difference in the amount of reflected light-flux between the wavelength ranges covered by a broad-band filter, while the specific features may cover a short spectral interval. Thus, the spectro-photometry is the first approximation of the spectral properties.

We were able to acquire spectro-photometric data for 2023 DZ_2 on the night 22 March 2023 using the Telescopio *Carlos Sánchez* (TCS) from Teide Observatory. Although these observations were performed after we acquired spectra using the GTC telescope, it is worth mentioning them as the first approach to infer the taxonomic classification in order to highlight the strength of this technique for fainter asteroids.

The observations were performed with the MuSCAT2[22] imaging instrument (Narita et al. 2019), which is mounted on the Cassegrain focus of the TCS. This configuration allows us to perform simultaneous photometric observations in four visible broad-band filters, namely g (400–550), r (550–700), i (700–820), and z_s (820–920) nm. At the end of each of the four channels there is an independently controllable CCD camera (1024×1024 pixels), having a pixel size of ∼0.44″ pixel^{-1} and a FoV of 7.4′ × 7.4′.

In order to obtain the light curves and the colours, we used the Photometry Pipeline (PP; Mommert 2017). This is a software package written in Python which obtains calibrated photometry from the FITS images by performing the astrometric registration, aperture photometry, photometric calibration, and asteroid identification. PP is written in Python and uses the *Astromatic* suite[23], namely SExtractor for source identification and aperture photometry (Bertin & Arnouts 1996), SCAMP for astrometric calibration (Bertin 2006), and SWarp for image re-gridding and co-addition (Bertin et al. 2002). It also uses the JPL Horizons module for obtaining the ephemerides of SSOs in order to identify them in the images.

[22] the acronym is derived from a multicolour simultaneous camera for studying atmospheres of transiting exoplanets.
[23] https://www.astromatic.net/

For astrometric registration, we used the *Gaia* DR2 catalogue (Gaia Collaboration 2018). In order to improve the accuracy, we applied the registration algorithm twice for each image. We discarded all those images for which the astrometric registration failed. The Pan-STARRS catalogue (Tonry et al. 2012) was used for all photometric calibrations. The accuracy of these calibrations is dependent on the number of stars imaged by each exposure (19 to 40 stars were used for the photometric calibration of each image).

The PP software uses aperture photometry performed by SExtractor. We applied the PP algorithm that finds the optimum aperture radius based on a curve-of-growth analysis (Howell 2000; Mommert 2017). From each set of four simultaneous images, we computed the $(g - r)$, $(r - i)$, and $(i - z_s)$ colours. The reported values of the colours represent the median of data obtained during 4 h of observations.

We used these colour values to infer the taxonomic classification. This was carried out in a robust way with the K-Nearest Neighbours (KNN) and Random Forest (RF) algorithms. These were implemented using the `Python` package `SCIKIT-LEARN`. The KNN algorithm classifies an object based on the label values or taxonomy of its neighbours in the colour-colour diagram, while the RF algorithm assigns the final label to an object using decision-tree structures.

Both algorithms require a training set that includes objects for which we know both the photometric colours (from our dataset) and spectral data (from the literature). To generate it we searched for the available spectral information of all the objects with TCS colours in the SMASS-MIT-Hawaii Near-Earth Object Spectroscopic Survey (MITHNEOS MIT-Hawaii Near-Earth Object Spectroscopic Survey) programme (Binzel et al. 2019) and the Modeling for Asteroids (M4AST) database (Popescu et al. 2012). We retrieved spectral classifications for 84 of the NEAS observed as well by our TCS/MuSCAT2 programme (Popescu et al. 2021). To increase the training sample, we computed the synthetic colours using the visible spectra published by Popescu et al. (2019) and Perna et al. (2018). The final training sample consisted of 154 asteroids classified as 5 A-types, 8 V-types, 34 Q-types, 48 S-complex, 7 B-types, 15 C-complex, 9 D-types, and 28 X-complex.

In order to account for magnitude errors determined on each of the broad-band filters, we applied a Monte Carlo approach. We started from the colour value and its error and generated three normal distributions (one for each colour) of 10 000 fictitious colour values. Then, for each of these cases we classified the object. Finally, the assigned taxonomy was the one with the highest frequency. Based on the colour values of $(g - r) = 0.555 \pm 0.055$ mag, $(r - i) = 0.154 \pm 0.055$ mag, and $(i - z_s) = 0.064 \pm 0.059$ mag, both algorithms classify this object as an X-complex (Fig. 8) member with 100% probability (this probability indicates that all the clones generated within the Monte Carlo approach were classified as X-complex objects).

The most powerful technique used to characterize this object was spectroscopy. The visible spectra of 2023 DZ_2 were obtained on two separate nights, first on the night of 17 March 2023 and again on the night of 20 March 2023, using the OSIRIS camera-spectrograph (Cepa et al. 2000; Cepa 2010) at the 10.4 m GTC, under the programme GTC31-23A. The telescope is located at the El Roque de Los Muchachos Observatory, on the island of La Palma (Canary Islands, Spain).

The OSIRIS instrument (upgraded in January 2023) was employed on both nights. We used the 1.2″ slit and the R300R grism (resolution R = 348 for a 0.6″ slit, dispersion of 7.74 Å pixel^{-1}) covering the 0.48–0.92 µm wavelength range.

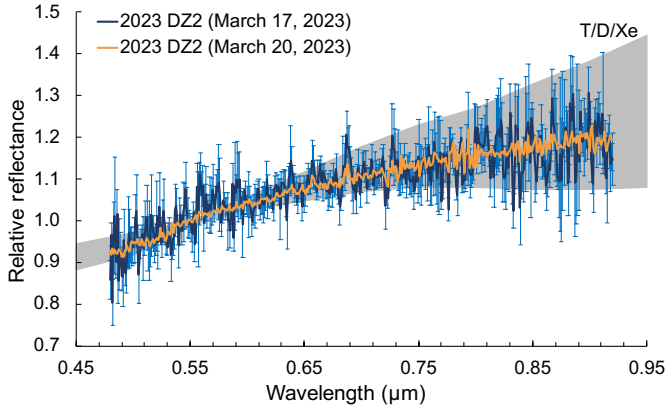

Fig. 9. Visible spectra of asteroid 2023 DZ_2 obtained with the 10.4 m Gran Telescopio Canarias on the night of 17 March 2023 (dark blue) and on the night of 20 March 2023 (orange). Error bars correspond to the standard deviation of the mean for the March 17 data. The error bars for the 20 March data are much smaller and are contained within the larger ones. The grey hatched region accounts for the three best taxonomic fits in order of increasing χ^2: T-, D-, and Xe-types.

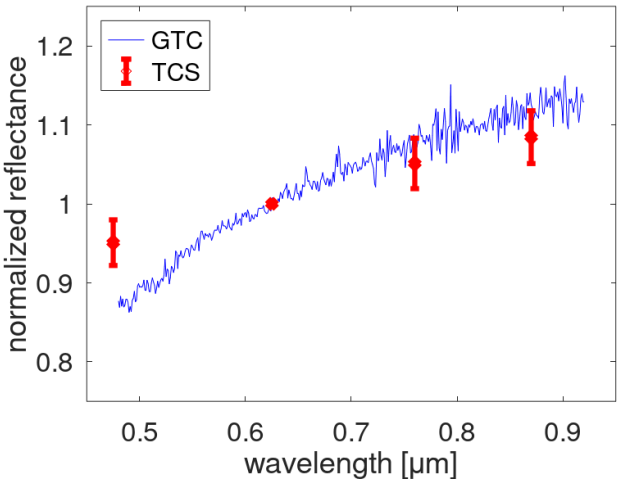

Fig. 10. Comparison between the spectra of 2023 DZ_2 obtained with GTC and the spectro-photometric data obtained with TCS. In order to convert the TCS data, the following colours of the Sun are used: $(g - r)^{\rm Sun} = 0.50$ mag, $(r - i)^{\rm Sun} = 0.10$ mag, $(i - z_s)^{\rm Sun} = 0.03$ mag. These values were derived by considering the profiles of the filters available for the MuSCAT2 instrument and are consistent with those provided by Holmberg et al. (2006).

The slit was oriented along the parallactic angle to minimize the effects of atmospheric differential refraction and the telescope tracking was set at the asteroid proper motion. Details of the observational circumstances are shown in Table 2. Two spectra of 300 s of exposure time each were obtained, with an offset of 10" in the slit direction in between them. To obtain the asteroid reflectance spectrum, we observed two solar analogue stars from the Landolt catalogue (Landolt 1992), SA98-978 and SA102-1081, at an airmass similar to that of the asteroid.

Data reduction was completed using standard procedures. The images were bias and flat-field corrected. Sky background was subtracted and a one-dimensional spectrum was extracted using a variable aperture, corresponding to the pixel where the intensity was 10% of the peak value. Wavelength calibration was carried out using Xe+Ne+HgAr lamps. This procedure was applied to the spectra of the asteroid and the stars. We then divided the asteroid's individual spectra by the spectra of the solar analogues, and the resulting ratios were averaged to obtain the final reflectance spectrum of 2023 DZ_2.

The spectrum obtained on the night of 17 March 2023 is shown in Fig. 9 in dark blue, together with the error bars associated with the standard deviation of the average. The spectrum obtained on the night of 20 March, when the asteroid was one apparent magnitude brighter, is shown in the same figure in orange. The agreement between the two spectra is perfect. Finally, the obtained spectra were used to classify 2023 DZ_2 taxonomically. We did so using the M4AST online tool[24]. The tool fits a curve to the data and compares it to the taxons defined by DeMeo et al. (2009) using a χ^2 fitting procedure. The three best results are provided in order of decreasing goodness of fit. For the case of 2023 DZ_2, the three best fits are T, D, and Xe (see hatched region in Fig. 9).

The T-types are defined by a linear spectrum with moderate to high slope at wavelengths below 0.75 μm by the Bus & Binzel (2002) and DeMeo et al. (2009) taxonomies. Their spectral curves are within the range of D-types and X-complex asteroids (comparable with the reddest X-types and with the least red D-types). For this reason, we did not include this spectral type among the classes used for spectro-photometric classification.

[24] http://spectre.imcce.fr/m4ast/index.php/index/home

The match between the spectral data and the spectro-photometry covers the r, i, and z_s bands (see Fig. 10).

There is a slight discrepancy (at the level of $2\sigma_g$, where σ_g is the standard deviation of the observations performed in the g filter). There are several factors that can contribute to it: (1) the g band covers the (0.4, 0.55) μm spectral interval, while the spectrum stops at 0.48 μm; (2) the common wavelength range between 0.48 and 0.55 μm falls on the outermost boundary of the spectroscopic setup coverage, making it more susceptible to potential unaccounted errors in the slope; (3) errors that have not been taken into account could arise either from the photometric calibration or from the spectral data, such as issues similar to those reported by Marsset et al. (2020) (although they refer to the near-infrared). With the existing data we cannot distinguish between these possibilities.

6. Discussions and conclusions

In the previous sections we have presented a comprehensive analysis of ground-based observations of a close-approaching NEA, namely 2023 DZ_2. All these analyses would provide critical information for making decisions on mitigating strategies regarding a hypothetical impact (either on impact avoidance or damage limitation) should this NEA have any real impact risk.

Our discovery of 2023 DZ_2 (initially classified as VI) with WFC mounted on INT, highlights the importance of continuous monitoring of the sky and the need to process the data in near real time. We showed that our ParaSOL infrastructure and the use of a synthetic tracking algorithm allowed us to process the large amount of data obtained and to report our findings in near real time so the community could start contributing additional observations of the object of interest as early as possible.

Once a potential impactor has been identified, it becomes critical to follow it up in order to improve its orbital determination and to obtain its physical properties, such as size, shape, composition, and structure. The size estimation requires knowledge of the absolute magnitude and the albedo (Harris & Harris 1997). The preliminary value of H can be inferred from the

apparent magnitude reported together with the astrometric measurements, after the orbit is computed. Nevertheless, this is a rough guess. The main source of the absolute magnitude errors is the irregular shape of the asteroids which generates light curves with amplitudes up to ≈2 mag, according to the current data existing in LCDB (Warner et al. 2009).

Thus, the photometric observations are the next step in characterizing the new NEA. In the case of 2023 DZ_2, we triggered observations with the TTT telescopes which revealed a rotation period of $P_{\rm rot} = 6.2743 \pm 0.0005$ min and an amplitude of 0.57± 0.14 mag. This result revealed a fast-rotating object. The minimum aspect ratio for its shape was estimated from the light curve amplitude, $a/b = 1.30 \pm 0.08$ (where a and b are the axis perpendicular to the rotation axis). Again, this was an approximate determination because the three peaks in the light curve outlined a body with a complex shape. Because this is a fast rotator, this finding added a limit on the cohesive strength of the material it is made of, and allowed us to constrain the possible solutions for size and composition.

The value of the albedo is strongly dependent on the composition of the body (Thomas et al. 2011; Mainzer et al. 2011; Popescu et al. 2018). It may vary in the interval of ≈(0.02, 0.50). In the case of 2023 DZ_2 and for the initial estimate of $H \approx 24$ mag and this wide range of albedos, we can estimate a size between 30 to 150 m. The albedo estimation can be made by assigning a taxonomic type. The most readily available technique for taxonomic classification is spectro-photometry, even if the obtained result is not as precise as that obtained from spectroscopy. The observational results obtained with TCS allowed us to classify 2023 DZ_2 as an X-complex asteroid; the colour values $(g - r) = 0.555 \pm 0.055$ mag, $(r - i) = 0.1542 \pm 0.055$ mag, and $(i - z_s) = 0.0638 \pm 0.059$ mag place this object well inside the X-complex locus in the colour-colour diagram.

Unfortunately, the tentative classification as an X-complex type NEA does not constrain the albedo, although this approach would have been successful for all the other classes. The X-complex includes both low- and high-albedo asteroids, with moderate spectral slope and featureless spectra, including various compositions similar to the carbonaceous, metallic, and enstatite chondrites (Fornasier et al. 2011). In the classification scheme of Tholen (1984), the X-complex was divided into three classes, primitives (P) ($p_V \approx 0.05$), metallics (M) ($p_V \approx 0.015$), and enstatites (E) ($p_V \approx 0.42$).

With this information, there are several hints regarding the nature of 2023 DZ_2. Because it is a fast rotator, we show that it is highly unlikely to have a carbonaceous composition that corresponds to a dark albedo (Licandro et al. 2023). This consideration reduced the possible interval for its size to the range from 33 to 55 m (assuming an albedo of 0.42 and 0.15, respectively). Accurate spectra can confirm this classification and eventually reveal subtle features that may allow us to determine its actual composition.

However, in order to obtain the visible spectrum, one must take into account that a 2.5 m class telescope is required for asteroids as faint as $V = 18.5$ mag (e.g. Popescu et al. 2019); a 4 m class telescope is needed for objects as faint as $V = 20.5$ mag (e.g. Perna et al. 2018); and a 10 m class telescope, such as GTC, the largest optical single-mirror telescope currently available, is required for bodies of $V \approx 22$ mag (e.g. de la Fuente Marcos et al. 2023). Within our effort to characterize 2023 DZ_2, we used the 10.4 m GTC telescope during the nights of 17 March and 20 March to obtain spectra over the 0.46–0.92 µm spectral range. The observations were performed when the object had respective apparent V magnitudes of 19 and 18. The two spectral curves are identical and show a featureless spectrum with a moderate slope. The agreement between them and the spectro-photometric observations is shown in Fig. 10.

In this paper we have described the first critical steps required to mitigate the threat of a potential impactor. We first detected 2023 DZ_2 using a near-real-time processing algorithm, within the context of a limited survey in a region of the sky not covered by the large surveys. As a second step, less than seven days after the announcement of its discovery by the Minor Planet Center (on 16 March 2023), we were able to constrain its main physical properties using photometric observations (acquired a few days later, during 20, 21, and 22 March), spectro-photometric data (obtained on 22 March 2023), and spectroscopic data (observations performed on 17 and 20 March). Regarding the origin of this NEA, its current orbit determination is not robust enough to determine which asteroid population is its most likely source; however, it is good enough to confirm that we are in no short-term danger of having a collision with 2023 DZ_2 thanks to the dynamical effects of a near secular (apsidal) resonance with Jupiter. This circumstance illustrates the dual nature of secular resonances, while ν_6 might place asteroids in a collision course with Earth and the nodal resonance with Earth favours collisions, ν_5 might help in protecting Earth from some impacts. In the case of the object studied here, the protective secular near resonance effectively removes the risk connected with the nodal near resonance.

Although simulated scenarios for a potential impact were carried out during Planetary Defense Conferences in 2021 and 2023 (Barbee et al. 2021), and they were much more elaborated, here we confirm on a real case that key observations can be obtained within a few days of the announcement of a potential impact threat. This time the data collected eventually helped to confirm that the collision probability was insignificant; next time this may not be the case: additional data may indicate a future impact instead. As the adage goes: Time is of the essence when mitigating a cosmic hazard.

Acknowledgements. The work of M.P., O.V., M.S., D.B., L.C. and M.P., was supported by a grant of the Romanian National Authority for Scientific Research – UEFISCDI, project number PN-III-P2-2.1-PED-2021-3625. RdlFM and CdlFM thank S.J. Aarseth for providing one of the codes used in this research and A.I. Gómez de Castro for providing access to computing facilities. This work was partially supported by the Spanish 'Agencia Estatal de Investigación (Ministerio de Ciencia e Innovación)' under grant PID2020-116726RB-I00 /AEI/10.13039/501100011033. Based on observations made with the Isaac Newton Telescope (INT), in the Spanish Observatorio del Roque de los Muchachos of the Instituto de Astrofísica de Canarias (program ID INT99-MULTIPLE-2/23A). Based on observations made with the Gran Telescopio Canarias (GTC), installed at the Spanish Observatorio del Roque de los Muchachos of the Instituto de Astrofísica de Canarias, on the island of La Palma. This work is partly based on data obtained with the instrument OSIRIS, built by a Consortium led by the Instituto de Astrofísica de Canarias in collaboration with the Instituto de Astronomía of the Universidad Nacional Autónoma de Mexico. OSIRIS was funded by GRANTECAN and the National Plan of Astronomy and Astrophysics of the Spanish Government.This paper includes observations made with the Two meter Twin Telescope (TTT) at the IAC's Teide Observatory that Light Bridges, SL, operates on the Island of Tenerife, Canary Islands (Spain). The Observing Time Rights (DTO) used for this research at the TTT have been provided by the Instituto de Astrofísica de Canarias. The spectral and the spectro-photometric data were obtained in the framework of the European Union's Horizon 2020 research and innovation program under grant agreement No 870403 (NEOROCKS). JL, JdeL, M.R-A and MP acknowledge support from the ACIISI, Consejería de Economía, Conocimiento y Empleo del Gobierno de Canarias and the European Regional Development Fund (ERDF) under grant with reference ProID2021010134. In preparation of this paper, we made use of the NASA Astrophysics Data System, the ASTRO-PH e-print server, and the MPC data server. We thank the reviewers for their comments which helped us to improve the paper. We also thank to Dr. Hissa Medeiros for the discussions on this topic and for the suggested references, to Gabriel Nicolae Simon for providing the python functions used for the spectro-photometric classification.

References

Aarseth, S. J. 2003, Gravitational *N*-Body Simulations (Cambridge, UK: Cambridge University Press)
Akhlaghi, M., & Ichikawa, T. 2015, ApJS, 220, 1
Alarcon, M. R., Licandro, J., Serra-Ricart, M., et al. 2023, PASP, 135, 055001
Barbee, B. W., Chodas, P., Dotson, J., et al. 2021, in 7th IAA Planetary Defense Conference, 57
Bertești eanu, D., Popescu, M., Mihai Gherase, R., et al. 2022, in European Planetary Science Congress, EPSC2022-1222
Bertin, E. 2006, ASP Conf. Ser., 351, 112
Bertin, E., & Arnouts, S. 1996, A&AS, 117, 393
Bertin, E., Mellier, Y., Radovich, M., et al. 2002, ASP Conf. Ser., 281, 228
Binzel, R. P., DeMeo, F. E., Turtelboom, E. V., et al. 2019, Icarus, 324, 41
Borovička, J., Spurný, P., Brown, P., et al. 2013, Nature, 503, 235
Brown, P. G., Assink, J. D., Astiz, L., et al. 2013, Nature, 503, 238
Bus, S. J., & Binzel, R. P. 2002, Icarus, 158, 146
Cepa, J. 2010, Ap&SS Proc., 14, 15
Cepa, J., Aguiar, M., Escalera, V. G., et al. 2000, SPIE Conf. Ser., 4008, 623
Christensen, E., Larson, S., Boattini, A., et al. 2012, in AAS/Division for Planetary Sciences Meet. Abstr., 44, 210.13
Cochran, A. L., Levison, H. F., Stern, S. A., & Duncan, M. J. 1995, ApJ, 455, 342
de la Fuente Marcos, C., & de la Fuente Marcos, R. 2012, MNRAS, 427, 728
de la Fuente Marcos, C., & de la Fuente Marcos, R. 2015, MNRAS, 453, 1288
de la Fuente Marcos, R., de León, J., de la Fuente Marcos, C., et al. 2023, A&A, 670, A10
DeMeo, F. E., Binzel, R. P., Slivan, S. M., & Bus, S. J. 2009, Icarus, 202, 160
Denneau, L., Jedicke, R., Grav, T., et al. 2013, PASP, 125, 357
Devillepoix, H. A. R., Bland, P. A., Sansom, E. K., et al. 2019, MNRAS, 483, 5166
Eaton, J. W., Bateman, D., Hauberg, S., & Wehbring, R. 2021, GNU Octave version 6.3.0 manual: a high-level interactive language for numerical computations
Farnocchia, D., Reddy, V., Bauer, J. M., et al. 2022, PSJ, 3, 156
Fornasier, S., Clark, B. E., & Dotto, E. 2011, Icarus, 214, 131
Froeschle, C., & Scholl, H. 1989, Celest. Mech. Dyn. Astron., 46, 231
Gaia Collaboration (Brown, A. G. A., et al.) 2018, A&A, 616, A1
Ginsburg, A., Sipőcz, B. M., Brasseur, C. E., et al. 2019, AJ, 157, 98
Giorgini, J. 2011, in Journées Systèmes de Référence Spatio-temporels 2010, ed. N. Capitaine, 87
Giorgini, J. D. 2015, in IAU General Assembly, 29, 2256293
Gladman, B., & Kavelaars, J. J. 1997, A&A, 317, L35
Gladman, B., Kavelaars, J. J., Nicholson, P. D., Loredo, T. J., & Burns, J. A. 1998, AJ, 116, 2042
Harris, A. W., & Harris, A. W. 1997, Icarus, 126, 450
Holmberg, J., Flynn, C., & Portinari, L. 2006, MNRAS, 367, 449
Howell, S. B. 2000, Handbook of CCD Astronomy
Ito, T., & Ohtsuka, K. 2019, Monogr. Environ. Earth Planets, 7, 1
James, S., Chandran, S. R., Aswathi, J., et al. 2022, Planet. Space Sci., 222, 105575
Kaiser, N. 2004, SPIE Conf. Ser., 5489, 11
Kartashova, A. P., Popova, O. P., Glazachev, D. O., et al. 2018, Planet. Space Sci., 160, 107
Kenkmann, T., & Artemieva, N. 2021, Meteor. Planet. Sci., 56, 1024
Kozai, Y. 1962, AJ, 67, 591
Landolt, A. U. 1992, AJ, 104, 340
Lang, D., Hogg, D. W., Mierle, K., Blanton, M., & Roweis, S. 2010, AJ, 139, 1782
Licandro, J., Popescu, M., Tatsumi, E., et al. 2023b, MNRAS, 521, 3784
Lidov, M. L. 1962, Planet. Space Sci., 9, 719
Mainzer, A., Grav, T., Bauer, J., et al. 2011, ApJ, 743, 156
Makino, J. 1991, ApJ, 369, 200
Marsset, M., DeMeo, F. E., Binzel, R. P., et al. 2020, ApJS, 247, 73
Milani, A. 2005, in IAU Colloq. 197: Dynamics of Populations of Planetary Systems, eds. Z. Knežević, & A. Milani, 219
Milani, A., Chesley, S. R., Boattini, A., & Valsecchi, G. B. 2000, Icarus, 145, 12
Mommert, M. 2017, Astron. Comput., 18, 47
Monteiro, F., Silva, J. S., Tamayo, F., Rodrigues, T., & Lazzaro, D. 2020, MNRAS, 495, 3990
Morbidelli, A., & Henrard, J. 1991, Celest. Mech. Dyn. Astron., 51, 169
Morrison, D. 1992, in The Spaceguard survey : report of the NASA International Near-Earth-Object Detection Workshop/David Morrison (Pasadena: Jet Propulsion Laboratory/California Institute of Technology)
Murray, C. D., & Dermott, S. F. 1999, Solar system dynamics (Cambridge, UK: Cambridge University Press)
Narita, N., Fukui, A., Kusakabe, N., et al. 2019, J. Astron. Telescopes Instrum. Syst., 5, 015001
Perna, D., Barucci, M. A., Fulchignoni, M., et al. 2018, Planet. Space Sci., 157, 82
Popescu, M., Birlan, M., & Nedelcu, D. A. 2012, A&A, 544, A130
Popescu, M., Licandro, J., Carvano, J. M., et al. 2018, A&A, 617, A12
Popescu, M., Vaduvescu, O., de León, J., et al. 2019, A&A, 627, A124
Popescu, M., de León, J., Licandro, J., et al. 2021, in European Planetary Science Congress, EPSC2021-820
Pravec, P., & Harris, A. W. 2000, Icarus, 148, 12
Reddy, V., Kelley, M. S., Farnocchia, D., et al. 2019, Icarus, 326, 133
Reddy, V., Kelley, M. S., Dotson, J., et al. 2022, The Planetary Science Journal, 3, 123
Rondón, E., Lazzaro, D., Rodrigues, T., et al. 2020, PASP, 132, 065001
Sánchez, P., & Scheeres, D. J. 2014, Meteor. Planet. Sci., 49, 788
Stănescu, M. & Văduvescu, O. 2021, Astron. Comput., 35, 100453
Stănescu, M., Popescu, M., Văduvescu, O., et al. 2023, in Asteroids, Comets, Meteors Conference
Tholen, D. J. 1984, PhD thesis, University of Arizona, USA
Thomas, C. A., Trilling, D. E., Emery, J. P., et al. 2011, AJ, 142, 85
Tonry, J. L., Stubbs, C. W., Lykke, K. R., et al. 2012, ApJ, 750, 99
Tonry, J. L., Denneau, L., Heinze, A. N., et al. 2018, PASP, 130, 064505
Vaduvescu, O., Popescu, M., Comsa, I., et al. 2013, Astron. Nachr., 334, 718
Vaduvescu, O., Curelaru, L., Popescu, M., Danila, B., & Ciobanu, D. 2020, A&A, 642, A35
Vaduvescu, O., Barwell, F., Jhass, K., et al. 2023, Minor Planet Electronic Circulars, 2023-F12
Valsecchi, G. B., Milani, A., Gronchi, G. F., & Chesley, S. R. 2003, A&A, 408, 1179
VanderPlas, J. T. 2018, ApJS, 236, 16
von Zeipel, H. 1910, Astron. Nachr., 183, 345
Warner, B. D., Harris, A. W., & Pravec, P. 2009, Icarus, 202, 134
Whidden, P. J., Bryce Kalmbach, J., Connolly, A. J., et al. 2019, AJ, 157, 119
Yanagisawa, T., Kamiya, K., & Kurosaki, H. 2021, PASJ, 73, 519
Ye, Q., Masci, F. J., Lin, H. W., et al. 2019, PASP, 131, 078002

Appendix A: Pro-Am collaborations for photometric characterization

Events that require rapid response observations or long-term monitoring campaigns of diverse celestial sources are the triggers for the collaboration between professional and amateur astronomers who have access to highly reliable observing facilities.[25] During its close approach, 2023 DZ_2 was bright enough for observations with small aperture telescopes. Thus, the light curves obtained initially could be followed up by many amateur astronomers.

We received various contributions from different amateurs from all over the world, including Amadeo Aznar, Lucian Hudin, and Cristian Suciu (Astroclubul Bucureşti, Romania). To highlight the importance of Pro-Am collaborations, we present here some of the most reliable light curves we received (Fig. A.1) and obtained by the *Isaac Aznar* Observatory (IAO) Alcublas (MPC code Z95), Valencia province, Spain; ROASTERR-1 Observatory (MPC code L04), Cluj-Napoca, Romania; and T025-BD4SB (MPC code 073), Bucharest, Romania (Bertesteanu et al. 2022). We choose to present here the typical plots that can be obtained using commercially available tools, such as `MPOC Canopus` and `Tycho Tracker`. With help from these tools, experienced amateur astronomers can derive the spin properties of asteroids.

Photometric observations of 2023 DZ_2 were performed from the ROASTERR-1 observatory with the 0.3 m f/5 corrected Newtonian, a CCD camera with a KAF-8300 CCD chip cooled at -15^{o}C, and a clear filter. The calibration data were acquired immediately after the observations and consisted of 32 bias, 32 dark, and 32 flat frames. Two sets of observations were used, made of 104 images and 138 images, respectively, with an exposure time of 10 s for each individual image. The `Tycho Tracker` v10 was used for photometry. The obtained period was 0.1038 h (6.228 min) with an amplitude of 0.526 mag, as shown in Fig. A.1.

The *Isaac Aznar* Observatory (IAO) is privately owned by the Spanish amateur astronomer Amadeo Aznar Macías. It is located in Alcublas, Valencia province, at 900 m above the sea level, in one of the darkest night-skies of the Iberian Peninsula (limiting magnitude 21.8 mag arcsec^{-2}). The optical system consists of a remotely controlled 0.36 m Schmidt-Cassegrain F/10 Meade LX200 telescope. The CCD camera is a SBIG STL 11000, with 1.68 arcsec pixel^{-1} resolution (pixel binned ×3) and a square FoV of 37×24 arcmin^2. The light curve of 2023 DZ_2 was obtained using 274 photometric exposures from two nights (see Fig. A.1), 21 and 25 March. An exposure time of 30 s was used, and images were acquired during ≈2.2 h. The data reduction was performed using the `MPO Canopus` software.[26] The light curve shows a rotation period of 0.1046 h (6.276 min) with an error of 0.0001 h and an amplitude of 0.50 mag with an error of 0.08 mag.

The T025–BD4SB robotic telescope was built as a collaboration between amateur astronomers from the Astroclubul Bucureşti and the researchers from the Astronomical Institute of the Romanian Academy. The main components of this instrument are a ten-inch Newtonian telescope and a QHY 294M CMOS camera. T025–BD4SB is mounted on the roof of the old Bucharest Astronomical Institute building. This facility has the Minor Planet Center observatory code 073. The detection limit is around V=20 mag, and the median seeing is 2.8 arcsec.

Table B.1. Barycentric Cartesian state vector of 2023 DZ_2: components and associated 1σ uncertainties.

Component		value$\pm 1\sigma$ uncertainty
X (au)	=	$-9.718051175253550\times10^{-1}\pm1.99342196\times10^{-8}$
Y (au)	=	$5.157636594173508\times10^{-1}\pm9.69360581\times10^{-9}$
Z (au)	=	$-7.025348786300637\times10^{-4}\pm1.18266109\times10^{-8}$
V_X (au/d)	=	$-4.772825832549133\times10^{-3}\pm8.13837751\times10^{-10}$
V_Y (au/d)	=	$-1.954511508654970\times10^{-2}\pm2.94881778\times10^{-10}$
V_Z (au/d)	=	$2.660147805349922\times10^{-5}\pm3.86774841\times10^{-10}$

Notes. Data are referred to epoch JD 2460000.5, which corresponds to 0:00 on 25 February 2023, TDB (J2000.0 ecliptic and equinox). Source: JPL `Horizons`.

The observations of 2023 DZ_2 were performed on the night of 24 March 2023 (one night prior to the close approach between 2023 DZ_2 and Earth). Continuous exposures of 5 s each were acquired during ≈5 h. This short exposure time was considered because of its high apparent motion (30–40 arcsec per min during the observations). By using this exposure time, the trail left on the image by the NEA matches the typical seeing from Bucharest. The data reduction followed the same steps as those described above. The image pre-processing was carried out using the Pyraf package.[27] Because of the light pollution of Bucharest, a sky background removal algorithm was applied using the GNU Astronomy Utilities (Gnuastro) package (Akhlaghi & Ichikawa 2015). The results obtained with the T025-BD4SB were a rotation period $P_{\rm rot}$ = 6.2753 ± 0.005 min and an amplitude of 0.482 mag.

Appendix B: Input data

Here we include the barycentric Cartesian state vector of NEA 2023 DZ_2. This vector and its uncertainties were used to perform the calculations discussed above. For example, a new value of the X component of the state vector is computed as $X_c = X + \sigma_X\, r$, where r is an univariate Gaussian random number, and X and σ_X are the mean value and its 1σ uncertainty in Table B.1.

[25] https://www.nature.com/articles/s41550-023-01954-6
[26] https://minplanobs.org/BdwPub/php/displayhome.php
[27] https://iraf-community.github.io/pyraf.html

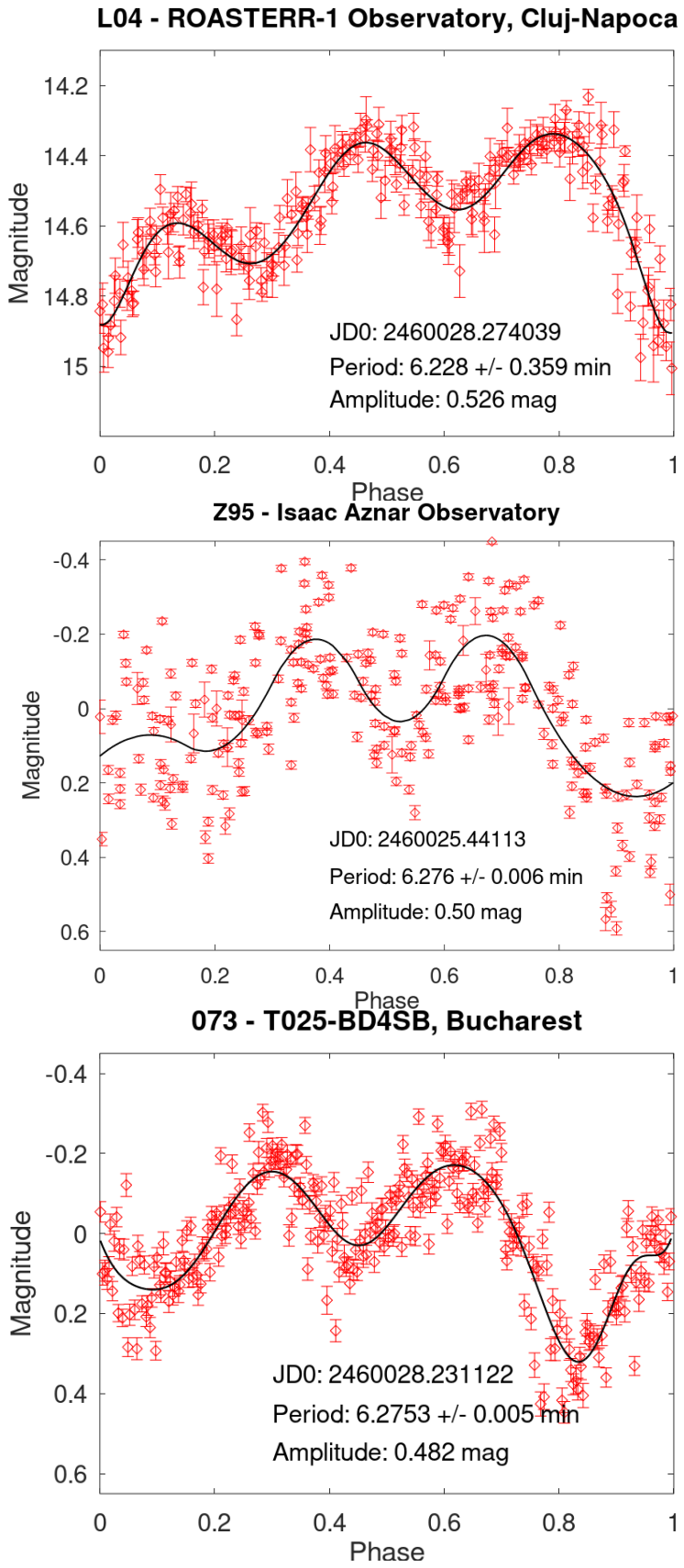

Fig. A.1. Phased light curve of 2023 DZ_2 computed using photometric measurements obtained within the Pro-Am collaboration discussed in the text. The title of each panel highlights the observatory (including the MPC code). The reported period and amplitude were computed by the observers using `Tycho Tracker` (for *L04* and *073*), and `MPO Canopus` (for *Z95*). The plots were made with GNU Octave software (Eaton et al. 2021), and a splinefit function was used to fit the data. In the case of 073, a binning of nine points was made after folding the photometric data.